Free-Carrier-Induced Ferroelectricity in Layered Perovskites

Shutong Li and Turan Birol

Phys. Rev. Lett. **127**, 087601 — Published 18 August 2021

DOI: 10.1103/PhysRevLett.127.087601

Free carrier induced ferroelectricity in layered perovskites

Shutong Li and Turan Birol*
Department of Chemical Engineering and Materials Science, University of Minnesota

(Dated: July 20, 2021)

Doping ferroelectrics with carriers is often detrimental to polarization. This makes the design and discovery of metals that undergo a ferroelectric-like transition challenging. In this letter, we show from first principles that the oxygen octahedral rotations in perovskites are often enhanced by electron doping, and this can be used as a means to strengthen the structural polarization in certain hybrid-improper ferroelectrics – compounds in which the polarization is not stabilized by the long range Coulomb interactions but is instead induced by a trilinear coupling to octahedral rotations. We use this design strategy to predict a cation ordered Ruddlesden-Popper compound that can be driven into a metallic ferroelectric-like phase via electrolyte gating.

Ferroelectrics, insulators with a spontaneous and switchable electric polarization, are promising for a wide range of applications and pose a number of fundamental questions [1–4]. While ferroelectricity is observed in a wide range of material classes and can be driven by a variety of mechanisms, the most studied ferroelectrics are transition metal oxides, such as $BaTiO_3$, where the emergence of a polar order parameter is due to a crystal structural distortion driven by the interatomic hybridization and long range Coulomb interactions [5, 6]. Because of the role of the long range interactions in driving the polar structural distortion, introduction of free charge carriers to ferroelectrics not only screens the ferroelectric polarization, but it also suppresses the structural distortion often [7].

While ‘structurally polar metals’ (metals with a polar point group) are rather common, ‘ferroelectric metals’ (metals that undergo a phase transition from a centrosymmetric to a polar crystal structure [8]) are rather rare. It took almost 50 years after the possibility of a ferroelectric-like transition in a metal was first raised [9] for the unambiguous experimental observation of such a transition in $LiOsO_3$ [10]. The first observation of polarization switching in a ferroelectric (semi-)metal is even more recent [11, 12]. The interest in polar and ferroelectric-like metals is continuing to increase in both bulk and heterostructures [13–24] and they continue to promise both a fertile playground for interesting emergent phenomena (including, but not limited to mixed singlet-triplet superconductivity [25] and novel optical effects[26]), and immediate relevance to applications as polar electrodes [27].

Emergence of polarization in (Sr,Ca)Ru_2O_6, $Ca_3Ru_2O_7$, and ultra-thin $NdNiO_3$ films have been studied in detail [28–30]; and it was shown that the polarization in these materials is robust against metalicity because the polar displacements are driven by their coupling to zone-boundary phonon modes and are mainly decoupled with the electrons around Fermi level. ‘Metallized ferroelectrics’ (insulating ferroelectrics that are doped to introduce charge carriers) are also studied intensively, and the effects of free carriers on the polarization and polar instabilities are analyzed recently introducing ideas such as metascreening [31], and elucidating the trends in the second-order Jahn-Teller effect under carrier doping [32]. Barring a volume expansion, the most common effect of charge doping in proper ferroelectrics is the suppression of the ferroelectric polarization; for example, ∼0.11 electrons per formula unit is sufficient to completely suppress the polarization in $BaTiO_3$ and render it centrosymmetric [7, 33, 34].

In this letter, we show that a particular group of ferroelectrics, the $A_3Sn_2O_7$ hybrid-improper ferroelectrics (HIFs) [35–39] behave differently, and their structural polarization is strongly enhanced by the free electrons introduced by chemical doping or electrostatic gating. This is related to an increase in the oxygen octahedral rotation angles induced by the added electrons in the parent perovskite compounds, which in turn leads to a larger structural polarization in these layered perovskite Ruddlesden-Popper (RP) phases [40]. We also show that it is possible to exploit this mechanism to obtain free carrier *induced* polarization, in other words, design a material that develops a ferroelectric-like structural instability when free electrons are introduced via, for example, electrostatic or electrolyte gating.

Oxygen Octahedral Rotations in Perovskites — We start by reviewing the symmetry and octahedral rotations in ABO_3 perovskites. Most perovskite oxides have the orthorhombic space group of $Pnma$ at low temperature [41]. The atomic displacements that lead to the $Pnma$ symmetry can be expanded in terms of the irreducible representations (irreps) of the reference space group $Pm\bar{3}m$ [42, 43]. The $Pnma$ structure has multiple nonzero strains (Γ_1^+, Γ_3^+, Γ_5^+) and atomic displacements (R_4^-, R_5^-, X_5^-, M_2^+, and M_3^+). Most of these distortions are ‘secondary’: they are nonzero only because of couplings with other, ‘primary’ distortions. The $Pnma$ structure can be obtained by a combination of only two primary irreps (R_5^- and M_3^+) which correspond to the out-of-phase and in-phase oxygen octahedral rotations shown in Fig. 1a-b [44]. Both of these space irreps are 3 dimensional, where the 3 orthogonal directions correspond to octahedral rotations around the

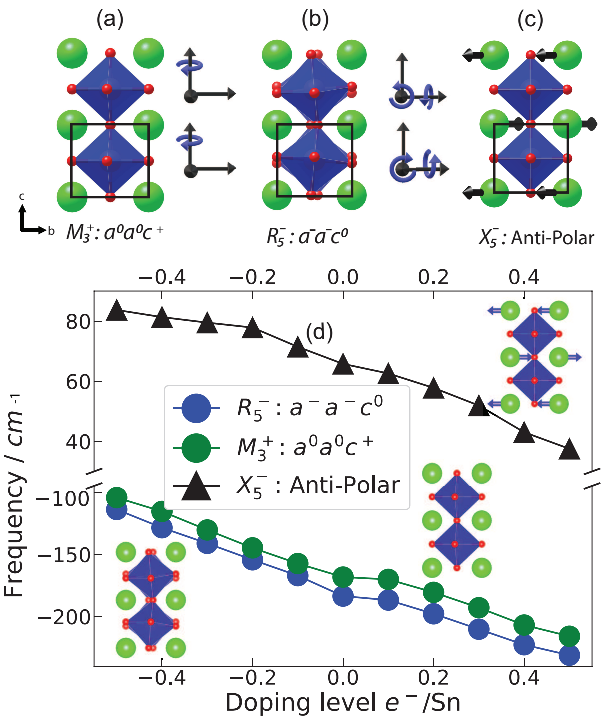

FIG. 1. (a)-(c)The three normal modes in Eq. 1 that are relevant to the $Pnma$ phase of perovskites and (d) (d) The phonon frequencies of cubic ($Pm\bar{3}m$) $SrSnO_3$ under doping and fixed volume. The green and red spheres represent the A-site and oxygen ions respectively, and the B-site atoms are in the center of the blue octahedra. (a) In-phase rotation around the c-axis ($a^0a^0c^+$ in Glazer notation). (b) Out-of phase rotation around the ab-axis $a^-a^-c^0$. (c) The anti-polar displacement in the ab-plane, where the irrep direction is $X_5^-(a,a;0,0;0,0)$. With increasing number of electrons, the unstable rotation modes get more unstable, and the anti-polar X_5^- mode gets softened (but remains stable).

three cubic axes. The phonons corresponding to both of these octahedral rotations are unstable in the cubic reference structure of $Pnma$ perovskites. The $Pnma$ structure ($a^-a^-c^+$ in the Glazer notation) has out-of-phase rotations around [110] and in-phase rotations around [001], which is equivalent to order parameter directions $R_5^-(a,a,0)$ and $M_3^+(0,0,a)$. These two modes, which we henceforth refer to as R and M for brevity, couple with the $X_5^-(a,a;0,0;0,0)$ mode (referred to as X for brevity) at the trilinear order. Hence, the Landau free energy up to third order is

$$\mathcal{F} = \alpha_R R^2 + \alpha_M M^2 + \alpha_X X^2 + \gamma R \cdot M \cdot X \qquad (1)$$

The X mode corresponds to an out-of-phase displacement of the A-site cations as showed in Fig. 1c, and is typically stable, but it has a nonzero amplitude $X = \gamma RM/2\alpha$ in the low temperature structure. X can be referred to as a 'hybrid-improper' order parameter, because it is induced in the ground state by a combination of two primary order parameters.

In heterostructures where translational symmetry is broken by layered cation ordering, or in layered perovskites (RPs), modes that give rise to transverse out-of-phase displacements of the A site (related to the X_5^- in perovskites) attain a polar character, and are responsible of the hybrid-improper ferroelectricity [35, 45, 46]. For this reason, understanding the behavior of this mode in bulk perovskites is essential for understanding the polarization trends in HIFs. As an example $Pnma$ perovskite system, we consider $SrSnO_3$. While $SrSnO_3$ is orthorhombic at room temperature, its Goldschmidt tolerance factor $t = \frac{R_{Sr}+R_O}{\sqrt{2}(R_{Sn}+R_O)} = 0.96$ is close enough to 1 so that it undergoes a series of phase transitions to the cubic phase above 1295 Kelvin and its structural ground state can be modified by biaxial strain [47, 48]. In Fig. 1(d), we show the phonon frequencies for the R, M, and the X modes as a function of doping from first principles DFT calculations. (The technical details of the calculations are discussed in the supplement [49].) The phonon frequencies are proportional to the square root of the α coefficients in Eq. 1, and can be used to study the instabilities. Unstable modes have imaginary frequencies, which are plotted as negative numbers. We simulate the effect of free carriers in this nominally insulating compound by changing the total number of electrons in the calculation, while keeping the system neutral by adding a homogeneous background charge. Unlike chemical substitution, this approach does not introduce any steric differences or disorder into the system. In this respect, it is a better representation of electrostatic or electrolyte gated systems rather than chemical doping. We consider a wide range of carrier doping up to 0.5 electrons per Sn atom, which is larger than the typical concentrations experimentally achievable [50]. We keep the unit cell volume fixed in order to separate out the volume expansion effects. The volume expansion does not modify the trends we report significantly [49].

The results in Fig. 1d show that both the rotation modes R_5^- and M_3^+, which have imaginary frequencies in the undoped compound, become more unstable with the introduction of free electrons, in other words, α_R and α_M become more negative with added electrons. Similarly, the frequency of the stable X_5^- mode decreases with increasing electron concentration, and so α_X becomes smaller. The trilinear coupling γ doesn't change significantly under doping, and the changes in the higher order coefficients are qualitatively insignificant [49]. As a result, the softening of X_5^- and the strengthening of the R_5^- and M_3^+ instabilities under electron doping lead to larger rotation angles and antipolar amplitudes as shown in Fig. 2. This trend is observed not only in $Pnma$ perovskites $SrSnO_3$ and $CaSnO_3$, but also in cubic perovskites like $BaZrO_3$, which develops a R_5^- instability when electron doped [49]. A similar enhancement of octahedral rotations was predicted by DFT in $SmNiO_3$ [51];

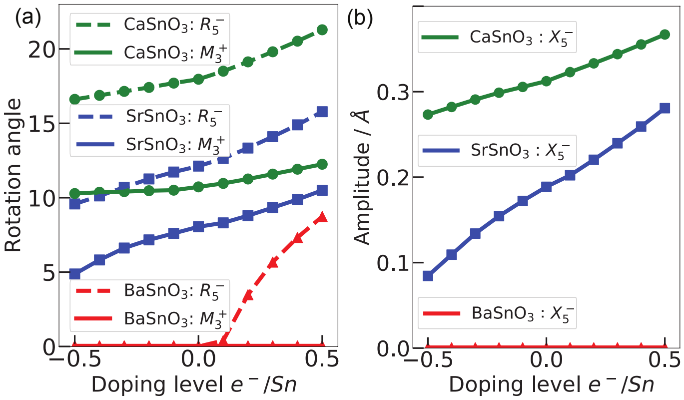

FIG. 2. Results of DFT structure optimizations under fixed volume. Both (a) the octahedral rotation angles (b) the anti-polar mode amplitudes increase with increasing number of electrons, as expected from the phonon frequencies in Fig. 1(d).

and both DFT and X-ray diffraction points to enhanced octahedral rotations in photodoped EuTiO$_3$ [52].

This effect of carriers on octahedral rotations can be explained by considering the densities of states. The valence bands in stannates consist of oxygen-p bands, whereas the the conduction band is formed by Sn-s [53]. The added electrons fill states with Sn-s character, and the valence of Sn^{4+} becomes Sn$^{+4-\delta}$. This decreases the Sn-O electrostatic attraction, decreases the Sn-O hybridization, and increases the ionic radius of Sn. This reduces the tolerance factor t. Added holes, on the other hand, occupy the O^{2-} anions and make them O$^{-2+\delta}$. This reduces the attraction between the A site cation (Ba, Sr, or Ca) and oxygens, which is the driving force of rotational instabilities. Hence, rotation modes become less unstable.

Hybrid-Improper Ferroelectrics — We now move on to A$_3$B$_2$O$_7$ HIFs, and consider Sr$_3$Sn$_2$O$_7$ as an example. Sr$_3$Sn$_2$O$_7$ is an $n = 2$ RP compound, which can be considered as a layered perovskite with an extra SrO layer after every pair of SrSnO$_3$ bilayers. It is experimentally verified to be a ferroelectric [36, 37], and its polarization is induced through the hybrid-improper mechanism which involves the trilinear coupling between the polar mode (Γ_5^-, which we denote as P) and two octahedral rotation modes (X_3^- and X_2^+, which we denote as Q_1 and Q_2) shown in Fig. 3a. These modes are the counterparts of the antipolar A-site displacement X_5^- mode, and the octahedral rotation modes R_5^- and M_3^+ in bulk perovskites. Two crucial differences between the A$_3$B$_2$O$_7$ RP and the ABO$_3$ perovskite structures are (i) in the smaller Brillouin zone of the RP structure, both the octahedral rotation modes Q_1 and Q_2 have the same wavevector, and hence can couple to zone center modes at the trilinear order, and (ii) the out-of-phase A-site displacement is now a polar Γ mode because the dipole moments in-

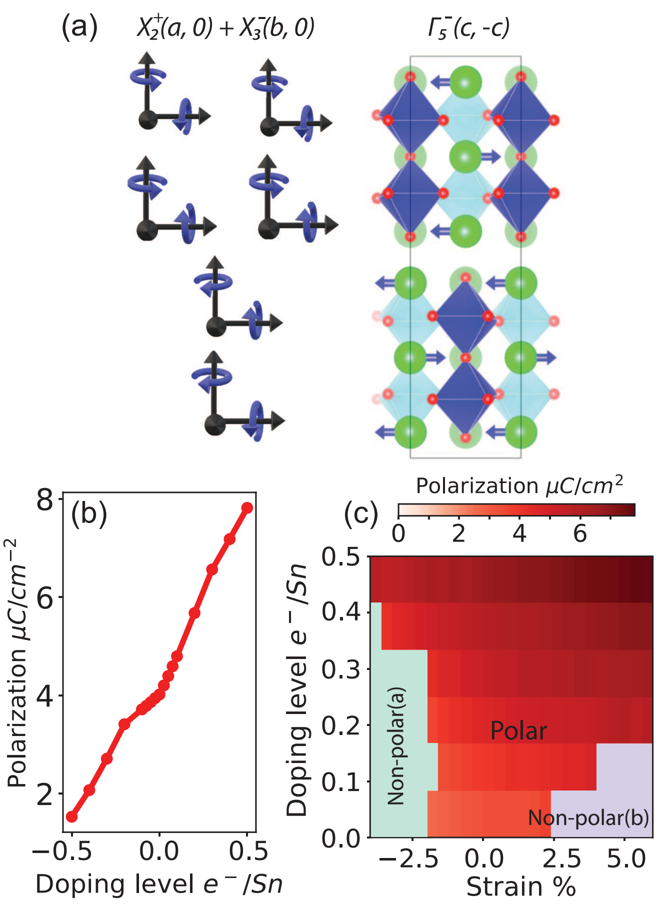

FIG. 3. (a) The structure of Sr$_3$Sn$_2$O$_7$ includes three structural distortion modes with respect reference $I4/mmm$ structure: Two oxygen octahedral rotation modes (X_2^+ and X_3^-) and a polar mode (Γ_5^-). (b) The structural polarization strength of Sr$_3$Sn$_2$O$_7$ as a function of doping level. The structural polarization is as the sum of the products of the nominal charge and polar displacements of ions [49]. (c) The doping – strain phase diagram of Sr$_3$Sn$_2$O$_7$. The non-polar(a) and non-polar(b) phases have $Aeaa$ and $P4_2/mnm$ space groups respectively [49].

duced by the symmetry inequivalent A-sites don't cancel. The shortest free energy that explains the polarization up to third order is

$$\mathcal{F} = \alpha_1 Q_1^2 + \alpha_2 Q_2^2 + \alpha_P P^2 + \gamma Q_1 Q_2 P \tag{2}$$

The trilinear coupling γ between the unstable Q_1 and Q_2 rotations with $\alpha_{1,2} < 0$ and the stable polar mode P with $\alpha_P > 0$ gives rise to a nonzero polarization $P = \gamma Q_1 Q_2 / 2\alpha_P$ in the groundstate.

In order to elucidate the change in the structural polarization in Sr$_3$Sn$_2$O$_7$ when free carriers are introduced, we optimize the crystal structure again with different numbers of added electrons or holes. The results in Fig. 3b show that added electrons increase the polarization, similar to the increased antipolar X mode amplitude in SrSnO$_3$. This can be explained by the fact that

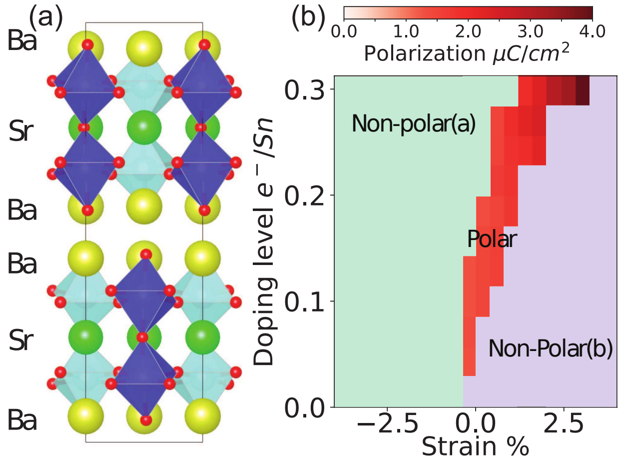

FIG. 4. (a) The structure and (b) a doping-strain phase diagram of $Ba_2SrSn_2O_7$. Yellow spheres represent Ba atoms. The non-polar(a) and non-polar(b) phases have $Aeaa$ and $P4_2/mnm$ symmetres respectively.

the mechanism that leads to enhancement of octahedral rotations in the electron doped $SrSnO_3$ is essentially a local mechanism that also applies to $Sr_3Sn_2O_7$, which also has a similar DOS with Sn-s bands on the conduction band. Filling the conduction band increases the effective ionic radius of the Sn ions, which in turn increases the amplitude of Q_1 and Q_2 octahedral rotations, and hence enhance the polarization P. In the HIF $Ca_3Ru_2O_7$ or the proper geometric ferroelectric-like $LiOsO_3$, the polarization is persistent against free carriers because of the absence of significant coupling between the electronic states near the Fermi level and the unstable phonons [28, 54]. In $Sr_3Sn_2O_7$, there is a strong effect of the conduction band occupation on the lattice instabilities, which is not reported in these other metallic ferroelectric-like compounds.

The enhanced rotations also expand the biaxial strain range where $Sr_3Sn_2O_7$ is structurally polar. In Fig. 3c, we show the strain – doping phase diagram of $Sr_3Sn_2O_7$, calculated by fixing the in-plane lattice parameters and relaxing the out-of-plane one to simulate the boundary conditions on a thin film lattice matched to a substrate. Insulating, undoped $Sr_3Sn_2O_7$ is known to undergo a transition to a non-polar phase above $\sim \mp 2\%$ biaxial strain [55] like many other compounds [56]. Fig. 3c shows that not only doping enhances polarization at fixed volume, but it also stabilizes the polar phase at wider strain ranges. The polar/non-polar transition induced by epitaxial strain is driven by the disappearance of one of two rotation modes in the polar phase [55]. The free electrons increase the stability of both rotation modes which make this phase transition occur at a higher strain value.

Ferroelectric-like transition induced by free electrons — The strong effect of free electrons on stabilizing a metallic ferroelectric-like phase in $Sr_3Sn_2O_7$ leads to the question *whether it is possible to drive a centrosymmetric compound to a polar phase by doping it with free electrons* without the help of biaxial strain. We scanned a number of $A_3B_2O_7$ oxides, but could not find an example that undergoes a polar phase transition for dopings up to 0.5 e^- per B site cation, which is already beyond what is experimentally achievable via methods such as electrostatic gating. In order to *design* a material which is closer to a structural phase transition than $Sr_3Sn_2O_7$, we turn to *targeted chemical pressure*, which involves selectively substituting part of Sr ions with larger Ba cations [57]. While it is not always possible to order same charge cations in bulk, molecular beam epitaxy has been successfully used to obtain targeted chemical pressure in other RP phases $(SrTiO_3)_n(BaTiO_3)_mSrO$ [57]. In $Sr_3Sn_2O_7$ ceramics, up to 10% of Ba ions are reported to preferentially substitute inequivalent Sr sites, however, the ordering tendencies depend sensitively on changes in the substitution amount [39]. We consider a structure where the 2/3 of Sr cations are substituted with Ba to form $Ba_2SrSn_2O_7$, where the Ba cations are on the double-rocksalt layers of the RP structure, as shown in Fig. 4a. While this structure is not energetically the most stable one [49], it may in principle be synthesized via layer-by-layer growth. The lowest energy structure of $Ba_2SrSn_2O_7$ is centrosymmetric when undoped and strain-relaxed, but introducing electrons to the conduction band leads to a transition to a polar structure with space group $Cmc2_1$ (Fig. 4b). Thus, $Ba_2SrSn_2O_7$ is a free carrier induced ‘metallic ferroelectric’. Like in undoped $A_3B_2O_7$ compounds, biaxial strain also modifies the stability range of the polar phase of $Ba_2SrSn_2O_7$.

Experimental verification of this prediction is possible. $Ba_3Sn_2O_7$ is stable in bulk [58], and thin films of both Sr and Ba stannate perovskites were grown by multiple groups [48, 59, 60]. If the free charge is constrained in the top ∼10 Å of a $Ba_2SrSn_2O_7$ film, the charge density needed to stabilize the polar phase is $\sim 5 \cdot 10^{13}$ cm^{-2}. Dielectric based gating allow densities of $\sim 10^{13}$ cm^{-2} [61], and it is possible to obtain densities exceeding $\sim 10^{14}$ cm^{-2} via ionic liquid gating [50, 62, 63]. Thus, it is possible to induce in-plane structural polarization electrolyte gating. The polarization can be observed by second harmonic generation as was done in $LiOsO_3$ [64].

Other $A_3B_2O_7$ compounds — This mechanism is very general, and it could be expected to be applicable to many other HIF oxides. However, our calculations on $Ca_3Ti_2O_7$ and $Sr_3Zr_2O_7$, which we discuss in the supplement [49] indicate that this is not the case. Even though the parent $CaTiO_3$ and $SrZrO_3$ compounds behave very similarly to $SrSnO_3$ under doping, the structural polarization of both $Ca_3Ti_2O_7$ and $Sr_3Zr_2O_7$ decrease upon electron doping. The reason is a subtle difference in the nature of polarization in these compounds: While both $Ca_3Ti_2O_7$ and $Sr_3Zr_2O_7$ have HIF groundstates, in their

$I4/mmm$ reference structure they also display weak polar Γ point instabilities [65, 66]. As a result of this instability, $Ca_3Ti_2O_7$ has a significant Ti contribution to polarization. This contribution is reduced as electrons are introduced to the system, because free carriers suppress the Ti–O hybridization and harden this soft mode in $Ca_3Ti_2O_7$ as they do in titanate perovskites $CaTiO_3$ or $BaTiO_3$ [7, 8, 49]. $Sr_3Sn_2O_7$, on the other hand, has no Γ instabilities, and has only a negligible SnO_2 layer polarization. This suggests the stannate perovskites as a unique group of compounds that can display free carrier enhanced (or induced) hybrid improper ferroelectricity.

Summary — Using first principles calculations and studying the oxygen octahedral rotations in $Pnma$ perovskites under doping, we showed that the structural polarization in stannate HIFs is not only robust against free carriers, but it is also enhanced. We furthermore predicted a yet-to-be-synthesized compound $Ba_2SrSn_2O_7$ that undergoes a centrosymmetric to polar transition under electron concentrations that are experimentally achievable by ionic liquid/gel gating. While our calculations are strictly at zero temperature and finding temperature dependence of lattice distortions requires molecular dynamics or effective Hamiltonian studies, the large energy gains we find suggest the possibility of observing this effect even at room temperature [49]. Our results show that the improper ferroelectricity driven by steric lattice instabilities can serve as a means to obtain carrier induced ferroelectricity in compounds where those instabilities are strengthened by the free carriers.

We acknowledge helpful suggestions of an anonymous Referee A for the discussion about $Ca_3Ti_2O_7$. This work was supported primarily by the National Science Foundation through the University of Minnesota MRSEC under Award Number DMR-2011401. We acknowledge the Minnesota Supercomputing Institute (MSI) at the University of Minnesota for providing resources that contributed to the research results reported within this paper.

---

[*] tbirol@umn.edu

[1] J. Dai, in *Ferroic Materials for Smart Systems* (Wiley, 2020) pp. 15–46.

[2] K. M. Rabe and P. Ghosez, Topics in Applied Physics **105**, 117 (2007).

[3] L. W. Martin and A. M. Rappe, Nature Reviews Materials **2**, 16087 (2017).

[4] J. F. Scott, Science **315**, 954 (2007).

[5] P. Ghosez, X. Gonze, and J. P. Michenaud, Europhysics Letters **33**, 713 (1996).

[6] R. E. Cohen, Nature **358**, 136 (1992).

[7] Y. Wang, X. Liu, J. D. Burton, S. S. Jaswal, and E. Y. Tsymbal, Physical Review Letters **109**, 1 (2012).

[8] N. A. Benedek and T. Birol, Journal of Materials Chemistry C **4**, 4000 (2016).

[9] P. W. Anderson and E. I. Blount, Physical Review Letters **14**, 217 (1965).

[10] Y. Shi, Y. Guo, X. Wang, A. J. Princep, D. Khalyavin, P. Manuel, Y. Michiue, A. Sato, K. Tsuda, S. Yu, M. Arai, Y. Shirako, M. Akaogi, N. Wang, K. Yamaura, and A. T. Boothroyd, Nature Materials **12**, 1024 (2013).

[11] Z. Fei, W. Zhao, T. A. Palomaki, B. Sun, M. K. Miller, Z. Zhao, J. Yan, X. Xu, and D. H. Cobden, Nature **560**, 336 (2018).

[12] P. Sharma, F.-X. Xiang, D.-F. Shao, D. Zhang, E. Y. Tsymbal, A. R. Hamilton, and J. Seidel, Science advances **5**, eaax5080 (2019).

[13] M. Meng, Z. Wang, A. Fathima, S. Ghosh, M. Saghayezhian, J. Taylor, R. Jin, Y. Zhu, S. T. Pantelides, J. Zhang, E. W. Plummer, and H. Guo, Nature Communications **10**, 1 (2019).

[14] H. J. Xiang, Physical Review B **90**, 094108 (2014).

[15] I. Lo Vecchio, G. Giovannetti, M. Autore, P. Di Pietro, A. Perucchi, J. He, K. Yamaura, M. Capone, and S. Lupi, Physical Review B **93**, 161113 (2016).

[16] H. M. Liu, Y. P. Du, Y. L. Xie, J. M. Liu, C. G. Duan, and X. Wan, Physical Review B - Condensed Matter and Materials Physics **91**, 2 (2015), 1409.4953.

[17] A. Narayan, Journal of Physics: Condensed Matter **32**, 125501 (2020).

[18] Y. R. Wang, S. Wang, H. L. Tao, Y. Cui, S. M. Liu, M. He, B. Song, and Z. H. Zhang, Solid State Communications **323** (2021), 10.1016/j.ssc.2020.114099.

[19] F. Jin, L. Wang, A. Zhang, J. Ji, Y. Shi, X. Wang, R. Yu, J. Zhang, E. W. Plummer, and Q. Zhang, Proceedings of the National Academy of Sciences **116**, 20322 (2019).

[20] J.-Y. Shan, A. de la Torre, N. J. Laurita, L. Zhao, C. D. Dashwood, D. Puggioni, C. X. Wang, K. Yamaura, Y. Shi, J. M. Rondinelli, and D. Hsieh, Physical Review Research **2**, 033174 (2020), 2008.00355.

[21] Z. Yimer and H. Fu, Physical Review B **101**, 174105 (2020).

[22] S. Ghosh, A. Y. Borisevich, and S. T. Pantelides, Physical Review Letters **119**, 177603 (2017).

[23] A. Zabalo and M. Stengel, Physical Review Letters **126**, 127601 (2021), 2007.11857.

[24] R. C. Xiao, D. F. Shao, W. Huang, and H. Jiang, Physical Review B **102**, 1 (2020), 2004.06913.

[25] S. Salmani-Rezaie, K. Ahadi, and S. Stemmer, Nano Letters **20**, 6542 (2020).

[26] V. P. Mineev and Y. Yoshioka, Phys. Rev. B **81**, 094525 (2010).

[27] D. Puggioni, G. Giovannetti, and J. M. Rondinelli, Journal of Applied Physics **124** (2018), 10.1063/1.5049607, arXiv:1611.06300.

[28] D. Puggioni and J. M. Rondinelli, Nature Communications **5**, 1 (2014), arXiv:1310.1148.

[29] T. H. Kim, D. Puggioni, Y. Yuan, L. Xie, H. Zhou, N. Campbell, P. J. Ryan, Y. Choi, J. W. Kim, J. R. Patzner, S. Ryu, J. P. Podkaminer, J. Irwin, Y. Ma, C. J. Fennie, M. S. Rzchowski, X. Q. Pan, V. Gopalan, J. M. Rondinelli, and C. B. Eom, Nature **533**, 68 (2016).

[30] S. Lei, M. Gu, D. Puggioni, G. Stone, J. Peng, J. Ge, Y. Wang, B. Wang, Y. Yuan, K. Wang, Z. Mao, J. M. Rondinelli, and V. Gopalan, Nano Letters **18**, 3088 (2018).

[31] H. J. Zhao, A. Filippetti, C. Escorihuela-Sayalero, P. Delugas, E. Canadell, L. Bellaiche, V. Fiorentini, and J. Íñiguez, Physical Review B **97**, 1 (2018).

[32] D. Hickox-Young, D. Puggioni, and J. M. Rondinelli, Physical Review B **102**, 1 (2020).

[33] T. Kolodiazhnyi, M. Tachibana, H. Kawaji, J. Hwang, and E. Takayama-Muromachi, Physical review letters **104**, 147602 (2010).

[34] C. Xia, Y. Chen, and H. Chen, Physical Review Materials **3**, 54405 (2019), arXiv:1905.13384.

[35] N. A. Benedek and C. J. Fennie, Physical Review Letters **106**, 107204 (2011).

[36] Y. Wang, F. T. Huang, X. Luo, B. Gao, and S. W. Cheong, Advanced Materials **29** (2017), 10.1002/adma.201601288.

[37] S. Yoshida, H. Akamatsu, R. Tsuji, O. Hernandez, H. Padmanabhan, A. Sen Gupta, A. S. Gibbs, K. Mibu, S. Murai, J. M. Rondinelli, V. Gopalan, K. Tanaka, and K. Fujita, J Am Chem Soc (2018), 10.1021/jacs.8b07998.

[38] J. J. Lu, X. Q. Liu, X. Ma, M. S. Fu, A. Yuan, Y. J. Wu, and X. M. Chen, Journal of Applied Physics **125**, 044101 (2019).

[39] B. H. Chen, T. L. Sun, X. Q. Liu, X. L. Zhu, H. Tian, and X. M. Chen, Applied Physics Letters **116** (2020), 10.1063/1.5138672.

[40] S. N. Ruddlesden and P. Popper, Acta Crystallographica **11**, 54 (1958).

[41] M. W. Lufaso and P. M. Woodward, Acta Crystallographica Section B: Structural Science **57**, 725 (2001).

[42] M. I. Aroyo and J. M. Perez-Mato, Acta Crystallographica Section A Foundations of Crystallography **54**, 19 (1998).

[43] B. J. Campbell, H. T. Stokes, D. E. Tanner, and D. M. Hatch, Journal of Applied Crystallography **39**, 607 (2006).

[44] P. M. Woodward, Acta Crystallographica Section B Structural Science **53**, 32 (1997).

[45] N. A. Benedek, J. M. Rondinelli, H. Djani, P. Ghosez, and P. Lightfoot, Dalton Transactions **44**, 10543 (2015).

[46] A. T. Mulder, N. A. Benedek, J. M. Rondinelli, and C. J. Fennie, Advanced Functional Materials **23**, 4810 (2013).

[47] M. Glerup, K. S. Knight, and F. W. Poulsen, Materials Research Bulletin **40**, 507 (2005).

[48] T. Wang, A. Prakash, Y. Dong, T. Truttmann, A. Bucsek, R. James, D. D. Fong, J.-W. Kim, P. J. Ryan, H. Zhou, T. Birol, and B. Jalan, ACS Applied Materials & Interfaces **10**, 43802 (2018).

[49] *See the supplemental information, which includes references [7, 8, 32, 55, 65-77], for details.*

[50] H. Yuan, H. Shimotani, A. Tsukazaki, A. Ohtomo, M. Kawasaki, and Y. Iwasa, Advanced Functional Materials **19**, 1046 (2009).

[51] M. Kotiuga and K. M. Rabe, Physical Review Materials **3**, 115002 (2019).

[52] M. Porer, M. Fechner, M. Kubli, M. J. Neugebauer, S. Parchenko, V. Esposito, A. Narayan, N. A. Spaldin, R. Huber, M. Radovic, E. M. Bothschafter, J. M. Glownia, T. Sato, S. Song, S. L. Johnson, and U. Staub, arXiv **012005**, 1 (2019), arXiv:1901.08388.

[53] H. Mizoguchi, H. W. Eng, and P. M. Woodward, Inorganic Chemistry **43**, 1667 (2004).

[54] N. J. Laurita, A. Ron, J.-Y. Shan, D. Puggioni, N. Z. Koocher, K. Yamaura, Y. Shi, J. M. Rondinelli, and D. Hsieh, Nature Communications **10**, 3217 (2019).

[55] T. Li, Shutong Birol, npj Computational Materials **6** (2020), 10.1038/s41524-020-00436-x.

[56] X. Z. Lu and J. M. Rondinelli, Nature Materials **15**, 951 (2016).

[57] N. M. Dawley, E. J. Marksz, A. M. Hagerstrom, G. H. Olsen, M. E. Holtz, V. Goian, C. Kadlec, J. Zhang, X. Lu, J. A. Drisko, R. Uecker, S. Ganschow, C. J. Long, J. C. Booth, S. Kamba, C. J. Fennie, D. A. Muller, N. D. Orloff, and D. G. Schlom, Nature Materials **19**, 176 (2020).

[58] Y. Hinatsu and K. Tezuka, Journal of Solid State Chemistry **138**, 329 (1998).

[59] A. Prakash, J. Dewey, H. Yun, J. S. Jeong, K. A. Mkhoyan, and B. Jalan, Journal of Vacuum Science & Technology A: Vacuum, Surfaces, and Films **33**, 060608 (2015).

[60] H. Paik, Z. Chen, E. Lochocki, A. Seidner H., A. Verma, N. Tanen, J. Park, M. Uchida, S. Shang, B.-C. Zhou, M. Brützam, R. Uecker, Z.-K. Liu, D. Jena, K. M. Shen, D. A. Muller, and D. G. Schlom, APL Materials **5**, 116107 (2017).

[61] A. Goldman, Annual Review of Materials Research **44**, 45 (2014).

[62] S. Z. Bisri, S. Shimizu, M. Nakano, and Y. Iwasa, Advanced Materials **29**, 1607054 (2017).

[63] C. Leighton, Nature Materials **18**, 13 (2019).

[64] H. Padmanabhan, Y. Park, D. Puggioni, Y. Yuan, Y. Cao, L. Gasparov, Y. Shi, J. Chakhalian, J. M. Rondinelli, and V. Gopalan, Applied Physics Letters **113**, 122906 (2018), arXiv:1809.05768.

[65] A. Mulder, *Ferroelectricity Coupled To Octahedral Rotations In Perovskite Oxides From First Principles*, Ph.D. thesis, Cornell University (2016).

[66] S. Yoshida, K. Fujita, H. Akamatsu, O. Hernandez, A. Sen Gupta, F. G. Brown, H. Padmanabhan, A. S. Gibbs, T. Kuge, R. Tsuji, S. Murai, J. M. Rondinelli, V. Gopalan, and K. Tanaka, Advanced Functional Materials **28**, 1801856 (2018).

[67] P. E. Blöchl, Physical review B **50**, 17953 (1994).

[68] G. Kresse and D. Joubert, Phys. Rev. B **59**, 1758 (1999).

[69] G. Kresse and J. Hafner, Phys. Rev. B **47**, 558 (1993).

[70] J. P. Perdew, A. Ruzsinszky, G. I. Csonka, O. A. Vydrov, G. E. Scuseria, L. A. Constantin, X. Zhou, and K. Burke, Phys. Rev. Lett. **100**, 136406 (2008).

[71] H. Stokes, D. Hatch, and B. Campbell, "Isotropy," (2007).

[72] P. Virtanen, R. Gommers, T. E. Oliphant, M. Haberland, T. Reddy, D. Cournapeau, E. Burovski, P. Peterson, W. Weckesser, J. Bright, S. J. van der Walt, M. Brett, J. Wilson, K. Jarrod Millman, N. Mayorov, A. R. J. Nelson, E. Jones, R. Kern, E. Larson, C. Carey, İ. Polat, Y. Feng, E. W. Moore, J. Vand erPlas, D. Laxalde, J. Perktold, R. Cimrman, I. Henriksen, E. A. Quintero, C. R. Harris, A. M. Archibald, A. H. Ribeiro, F. Pedregosa, P. van Mulbregt, and S. . . Contributors, Nature Methods **17**, 261 (2020).

[73] A. Filippetti, V. Fiorentini, F. Ricci, P. Delugas, and J. Íñiguez, Nature Communications **7**, 11211 (2016).

[74] E. A. Nowadnick and C. J. Fennie, Physical Review B **94**, 104105 (2016).

[75] N. A. Benedek and C. J. Fennie, Journal of Physical Chemistry C **117**, 13339 (2013).

[76] S. Ivantchev, E. Kroumova, G. Madariaga, J. M. Pérez-Mato, and M. I. Aroyo, Journal of Applied Crystallography **33**, 1190 (2000).

[77] T. Birol, N. A. Benedek, and C. J. Fennie, Physical

Review Letters **107**, 257602 (2011).